ROBOMECH Journal

RESEARCH ARTICLE

Open Access

Series admittance–impedance controller for more robust and stable extension of force control

Takuto Fujiki and Kenji Tahara*

Abstract

To control a robot performing cooperative work between a human and robot, not only the position but also the force must be controlled from the viewpoint of human–robot contact. In addition, when a robot is used for fitting and handling, tasks that are conventionally performed by experienced humans, controlling the grasping force and the force exerted by the joints can produce motions similar to those of humans and contribute to improving the success rate of the work. In the field of force control, in addition to direct force control, admittance control and impedance control are modes based on the relationship between position and force, which are known to be robust and safe. However, admittance control often becomes unstable when the robot comes into contact with a rigid body, and the performance of impedance control is degraded by friction. In this study, we aim to realize safe and accurate force control in cooperative work with humans. As a precursor, we propose admittance and impedance control, which is a series connection of conventional admittance control and impedance control. We show that the proposed force control is more robust, stable, and accurate than impedance control and admittance controls alone, or at least as good as them, when in contact with an unknown environment. Its basic effectiveness and practical usefulness are demonstrated through numerical simulations and experimental results.

Keywords: Force control, Admittance control, Impedance control, Stiffness ellipse, Numerical simulation, Experiment

Introduction

From the automobile to the food industry, the automation and robotization of many task types are attracting attention in various field. Generally, simple tasks requiring high speed or high power, such as automobile assembly or welding, are mainly performed by robotic systems, whereas other complicated tasks with high power, such as the installation of small parts or wiring, are mainly performed by humans. One of the reasons is that mainstream industrial robots are heavy and large, and the technology for handling fragile objects in precise tasks or adapting to unexpected contact has not yet matured. In the food industry, many manufacturing processes are performed by robots; however, the manipulation, sorting, and packing of soft foods are still performed by humans mainly because a process to control the manipulator to grasp and manipulate soft objects at a certain speed without injuring them has not been developed. In the field of industrial robotics, accidents must be avoided by installing safety measures between humans and robots because heavy-weighted robots move at high speed and high power. In recent years, human-collaborative robots have been developed, wherein humans and robots work in close proximity without a fence between them.

Human-collaborative robots must have a structural safety function and mechanism to detect unexpected contact with the environment. Various cooperative robots have been developed so far, however, most have a limitation in that the output of each actuator is saturated, and few have an algorithm to realize both high power and

*Correspondence: tahara@ieee.org

Department of Mechanical Engineering, Graduate School of Engineering, Kyushu University, 744 Moto'oka, Nishi-ku, Fukuoka 8190395, Japan

safety. To this end, the realization of softness from the viewpoint of hardware and software has been studied.

To handle soft objects, many studies have developed end-effectors using soft materials; some studies have used polymeric materials and air pressure to actuate the soft end-effector [1–3]. Renda et al. developed a soft robot that resembles an octopus leg using soft materials and presented a kinematic model that allows for complex motions such as bending and reaching [4]. Giannaccini et al. developed a cable-driven soft gripper that conforms to the shape of a grasped object and demonstrated the possibility of applying it to various objects [5]. Thus, an objective could be achieved using adequate soft materials for specific tasks and by devising structures from the viewpoint of hardware. However, there are difficulties in describing the accurate dynamics due to individual differences and a decrease in control accuracy due to the robot's own nonlinear dynamics, induced by the softness. Therefore, it is difficult to achieve high-accurate control performance with manipulators using soft materials. From the viewpoint of control design, robustly and safety regulating not only the position and velocity of the end-effector but also the contact force should be one of the important and desirable abilities of a manipulator. Several types of force controllers have been proposed so far, such as direct force feedback controllers, impedance controllers, and admittance controllers [6, 7]. Admittance and impedance controllers have been frequently used so far because their implementation is easy, and they can handle unknown objects stably without injuring the environment [8–10]. Although they have been useful in controlling contact forces in specific situations, for their use in general applications in the industry, there is still room for improvement in terms of robustness, stability, and accuracy. Impedance control regulates the output force of an end-effector based on the desired mechanical impedance parameters according to the input acceleration, velocity, and displacement at the end-effector. In impedance control, because the dynamics of the manipulator itself become one of the disturbances in achieving the desired mechanical characteristics, a nonlinear compensation method such as a computed torque method is often used. However, the control accuracy can easily deteriorate owing to model errors such as friction [11, 12]. Additionally, because the input is the displacement and velocity of the end-effector, an output force cannot be generated unless such displacement and velocity occur. Namely, singularity avoidance and back-drivability are important [13, 14].

In contrast, admittance control regulates the position, velocity, and acceleration of the end-effector based on the desired mechanical admittance parameters according to the contact force detected by the force sensor. In admittance control, there is a possibility that the desired position and velocity derived based on the contact force would diverge when the force sensor detects a sudden impulsive large force, for example, when in contact with a stiff environment. In such cases, the behavior of the manipulator becomes unstable [15, 16]. Furthermore, because the input is a contact force, it is impossible to respond to contact occurring in a location without a force sensor; in such a case, the manipulator becomes stiff because generally a high gain position controller is used in the final output stage of the admittance controller. A disturbance observer can estimate the contact force; however, an accurate model of the overall system is required [17]. In general, impedance control is relatively more stable than admittance control when in contact with stiff environments, and admittance control is relatively more accurate than impedance control when in contact with soft environments. However, in cases in which the contact environments are unknown and changeable in terms of mechanical and geometric properties, it is difficult to select which one to use in advance and also to achieve the desired mechanical characteristics using either of these methods.

To address this issue, Ott et al. combined admittance and impedance controllers in parallel to expand the usable frequency range by switching between them according to the environment [18]. However, such a mechanism requires fast switching between two controllers, which results in discontinuous inputs that may induce unstable behavior, and may not always be effective depending on environment and the desired mechanical characteristics. As a combination of force and position controllers, Anderson et al. proposed hybrid impedance control, which combines hybrid force/position control and impedance control, and successfully performed the peg-in-hole task in a two-dimensional simulation [19]. In this controller, a selection matrix is used to choose the force and position control subspaces in the hybrid control part, and an impedance controller is used as the final output stage of the controller; these two controllers are synthesized through a proxy. However, the process mainly focuses on the design of the input acceleration in the hybrid control part and the mechanical characteristics of the impedance control part, and it does not describe how to design the desired trajectory of the proxy during operation.

In this study, we propose force control method that integrates impedance and admittance controllers in series to exploit the advantages of both the controllers. The proposed controller realizes more robust and stable behavior than the two conventional force controllers when in contact with an unknown changeable environment. Additionally, an anisotropic endpoint stiffness

ellipse can be achieved in the design of the mechanical characteristics of impedance and admittance controls [20]. The elliptical design of the mechanical characteristics enables both securing of tracking performance by mechanical admittance and the suppression of vibrations in contact by mechanical impedance. First, a new force controller is designed. Second, its stability is analyzed to provide a guideline for designing the mechanical characteristics and is compared with that of conventional force controllers based on frequency analysis in a one-DoF system using Nyquist diagrams. Next, numerical simulations are conducted in which the stiffness of the contact environment in a one-DOF system is varied to verify its position accuracy and vibration suppression with changes in mechanical properties, and the effectiveness of the proposed controller is demonstrated in comparison with conventional force controllers. Subsequently, the practical usefulness of the proposed controller is demonstrated through experiments using a one-DOF experimental setup. Finally, the proposed method is extended to a two-DOF system, and a numerical simulation with the two-DOF system is conducted, in which the end-effector traces the contour of an unknown environment in contact in a 2D case. The effectiveness of the anisotropic endpoint stiffness ellipse designed in the proposed controller is demonstrated through numerical simulation results.

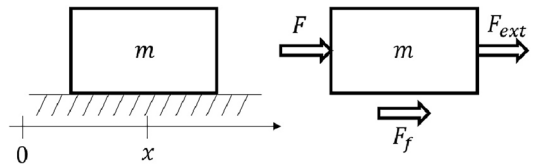

Fig. 1 One-dimensional system

Force control using the relationship between position and force

One-dimensional model

In this study, we first considered a force control system in a one-dimensional model, as shown in Fig. 1, where m denotes the mass, x denotes the position, F denotes the input force, and F_{ext} denotes the external force. The equation of motion for a one-dimensional system is as follows:

$$m\ddot{x} = F + F_{ext}. \tag{1}$$

Impedance control

Impedance control is a force control that outputs a set reaction force based on the displacement of the controlled object as the input. A block diagram of the impedance control is shown by the green dotted line in Fig. 2. Where x_0 denotes the desired position of the control object. As shown in Fig. 2, the output is derived from the difference between the current and desired positions of the control object. The motion (mechanical characteristics) of an object controlled by impedance control is represented by the following equation:

$$M_{\mathrm{d}}(\ddot{x} - \ddot{x}_0) + D_{\mathrm{d}}(\dot{x} - \dot{x}_0) + K_d(x - x_0) = F_{\mathrm{ext}} \tag{2}$$

From the above equation, the objective is to realize the response of the desired spring-mass-damper system to the external force applied to the control object. The design parameters are the desired inertia M_d, desired viscosity D_d, and desired stiffness K_d, which are included in Eq. (2). Next, we find the input to obtain the desired mechanical properties as shown in Eq. (2). From the equation of motion of the control object (Eq. 1), the control input F is expressed as follows:

$$F = m\ddot{x} - F_{\mathrm{ext}}. \tag{3}$$

When Eq. (3) is used as the input, we need to measure the acceleration $\ddot{x}$ of the target; however, because it is

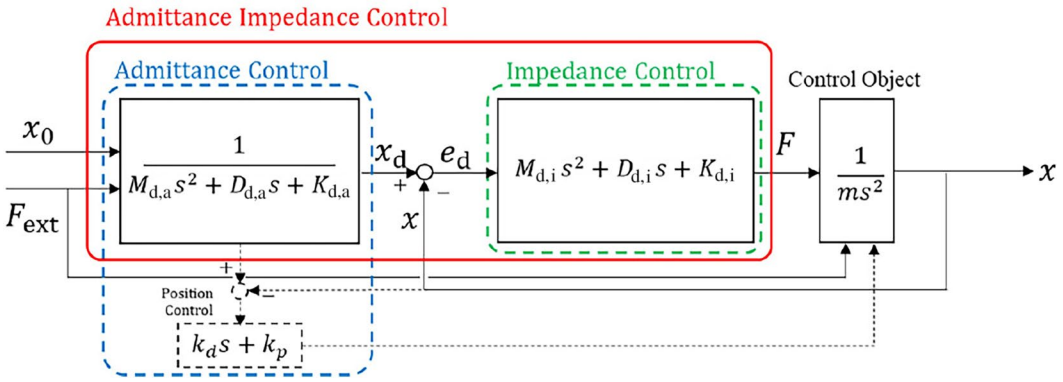

Fig. 2 Block diagram of the proposed control

difficult to measure the actual acceleration, we use Eq. (2) to replace the acceleration $\ddot{x}$ with

$$\ddot{x} = \frac{1}{M_\mathrm{d}} F_\mathrm{ext} + \ddot{x}_0 - \frac{1}{M_\mathrm{d}} (D_\mathrm{d}\dot{e} + K_\mathrm{d} e), \tag{4}$$

where $e = x - x_0$ and $\ddot{x}_0$ is the desired acceleration and need not be measured. Therefore, from Eqs. (3) and (4), the input for the impedance control is given as follows:

$$F = \left(\frac{m}{M_\mathrm{d}} - 1\right) F_\mathrm{ext} + m\ddot{x}_0 - \frac{m}{M_\mathrm{d}} (D_\mathrm{d}\dot{e} + K_\mathrm{d} e). \tag{5}$$

In impedance control, depending on the desired impedance, the control performance generally tends not to be unstable, even if the robot comes in contact with a stiff environment. As can be seen from Eq. (5), when the model of the object with the desired mechanical impedance m is close to the true value, and inertia due to the mass of the model can be eliminated depending on the value of M_d. Therefore, the motion of an object with the desired mechanical impedance, which is the motion desired by the designer, can be realized. However, because impedance control does not use force as an input, but only position and velocity, if the static frictional force acting on the system is equal to the force obtained as the output of the impedance control, the system may not reach the desired position x_0 and may settle at the local equilibrium point, which means that the control accuracy deteriorates. In addition, when it is introduced to a robot that does not have sufficient backdrivability, such as a robot with a high reduction ratio reducer, it may not be possible to generate sufficient displacement as an input.

Admittance control

Admittance control is a type of control method that allows a robot to follow external forces by calculating the desired position, velocity, and sometimes acceleration using the equation of motion of a virtual object in response to external forces. The block diagram of admittance control is indicated by the blue dotted line in Fig. 2.

$$\begin{aligned} &M_\mathrm{d}(\ddot{x}_\mathrm{d} - \ddot{x}_0) + D_\mathrm{d}(\dot{x}_\mathrm{d} - \dot{x}_0) + K_\mathrm{d}(x_\mathrm{d} - x_0) \\ &= F_\mathrm{ext}. \end{aligned} \tag{6}$$

where $e_d = x_d - x_0$ and x_d denotes the desired function obtained from Eq. (6). That is, Eq. (6) represents the motion of a virtual object with the mechanical properties (admittance) of the target. The external force F_{ext} acting on the control object is assumed to act on the virtual object, as represented by Eq. (6), and the desired position can be calculated by solving the equation of motion. The general admittance control uses a position controller with the desired position input, as shown in Fig. 2. If the position controller can make the control object follow the desired trajectory with high accuracy, the motion of the control object can be brought closer to that of the virtual object with the desired admittance characteristics. In this study, we used the following equation as a position controller to output force F, with the desired position x_d of the virtual object as an input.

$$F = k_p(x_\mathrm{d} - x) - k_v\dot{x}. \tag{7}$$

Substituting Eq. (7) into Eq. (1), the equation of motion for the control object is expressed as follows:

$$m\ddot{x} + k_v\dot{x} + k_p(x - x_\mathrm{d}) = F_\mathrm{ext}. \tag{8}$$

Admittance control realizes a response close to the desired admittance. In particular, when considering a relatively soft environment, the desired response can be stably realized because the desired trajectory according to the input force seems to remain around the present position and tends not to diverge. However, there are some problems, such as the fact that the input is a force, and thus, it can only respond to external forces obtained from the force sensor, which results in a loss of control accuracy owing to the delay and noise included in the force information.

Combining admittance control and impedance control

Combination of force control with switching

As a control method that combines the impedance and admittance control, Ott et al. developed a control method that combines impedance and admittance controls with switching [18]. They used admittance and impedance controls in parallel, and these controllers were alternatively used by switching according to the desired frequency, which is determined by the duty ratio n. The duty ratio should be adjusted to achieve the desired mechanical characteristics in a changeable external environment. The advantages of both admittance and impedance controls are adequately utilized according to the duty ratio. However, it is assumed that the external environment is known, including its changes, and adjustment of the duty ratio must be set in advance to determine the changes in the external environment. In addition, chattering may occur when implementing a discontinuous switching algorithms that sometimes induce instability.Therefore, in the next section, we propose a new force controller that demonstrates the advantages of both impedance and admittance controllers for unknown environments and does not use any discontinuous switching algorithms.

Admittance and impedance control

A block diagram of the control method that combines admittance and impedance control proposed in this study is shown in Fig. 2. This control method is hereinafter referred to as the admittance and impedance control method. The newly proposed admittance and impedance control method is completely different from the parallel switching method proposed by Ott et al. [18] in that the admittance control and impedance control are placed in series. When an external force acts on a control objective, the desired position and velocity are derived by solving the equation of motion of a virtual object that has the desired mechanical characteristics using admittance control. Subsequently, impedance control is used to realize the desired position and velocity derived through the admittance controller.

The advantage of the proposed method is that it is a single continuous controller; thus, a switching algorithm is not required, which eliminates the effects of chattering and other problems. In addition, the mechanical properties of the admittance control and impedance control can be set by each, which may enable stable control over a wide frequency range. Equations (9) and (10) below show the input/output relationship of the proposed controller.

Admittance control

$$M_{\mathrm{d,a}}\ddot{x}_{\mathrm{d}} + D_{\mathrm{d,a}}\dot{x}_{\mathrm{d}} + K_{\mathrm{d,a}}(x_{\mathrm{d}} - x_0) = F_{\mathrm{ext}} \tag{9}$$

Impedance control

$$\begin{aligned} F = &\left(\frac{m}{M_{\mathrm{d,i}}} - 1\right)F_{\mathrm{ext}} \\ &+ m\ddot{x}_d - \frac{m}{M_{\mathrm{d,i}}}\left(D_{\mathrm{d,i}}\dot{\hat{e}}_{\mathrm{d}} + K_{\mathrm{d,i}}\hat{e}_{\mathrm{d}}\right), \end{aligned} \tag{10}$$

where $\hat{e}_d = x_d - x$ and $\ddot{x}_d$ is the acceleration of the virtual object, which is the value calculated from Eq. (9), so there is no need to measure the acceleration by a sensor. In this study, the desired admittance ($M_{d,a}$, $D_{d,a}$, $K_{d,a}$) and the desired impedance ($M_{d,i}$, $D_{d,i}$, $K_{d,i}$) are given as constants.

Stability

To demonstrate that the proposed controller can achieve stable behavior under various external forces, the stability of the system is discussed. In this section, we first assume that the proposed method is used for a system with one degree of freedom and that the transfer function is obtained by the Laplace transform. Then, we discuss the stability region based on the impulse response obtained by the inverse Laplace transform of the transfer function.

Impulse response

We obtain a transfer function that includes the system when using the proposed method for a system with one-DOF. First, by Laplace transformation of Eq. (9), we obtain the transfer function of admittance control, where the input is an external force F_{ext} and the output is the position of the virtual object x_d.

$$(M_{d,a}s^2 + D_{d,a}s + K_{d,a})X_d = F_{ext} \tag{11}$$

$$\begin{aligned} X_d &= \frac{1}{M_{d,a}s^2 + D_{d,a}s + K_{d,a}}F_{ext} \\ &= G_a(s)F_{ext} \end{aligned} \tag{12}$$

where $X_d = \mathcal{L}[x_d(t)]$, and $G_a(s)$ represents the transfer functions of the admittance control. Next, assuming that the acceleration of the system can be measured, the input F to the system by impedance control is shown in Eq. (13), and the transfer function is obtained by Laplace transform as shown in Eq. (14).

$$M_{d,i}(\ddot{x}_d - \ddot{x}) + D_{d,i}(\dot{x}_d - \dot{x}) + K_{d,i}(x_d - x) = F \tag{13}$$

$$\begin{aligned} F(s) &= (M_{d,i}s^2 + D_{d,i}s + K_{d,i})(X_d - X) \\ &= G_i(s)(X_d - X) \end{aligned} \tag{14}$$

Here, $X = \mathcal{L}[x(t)]$, and Eq. (14) takes the difference between the position X of the system and the virtual desired position X_d as the input, and the force F applied to the system as the output. The equation of motion for a one-degree-of-freedom system is given by Eq. (1), and the Laplace transform of Eq. (1) yields Eq. (15).

$$mXs^2 = F(s) + F_{ext} \tag{15}$$

Substituting Eqs. (12) and (14) into Eq. (15), we obtain an input-output equation in which the input is the external force and the output is the system position, as shown in Eq. (17).

$$mXs^2 = G_i(s)(G_a(s)F_{ext} - X) + F_{ext} \tag{16}$$

$$\begin{aligned} X &= \frac{G_a(s) + G_i(s)}{\{(m + M_{d,i})s^2 + D_{d,i}s + K_{d,i}\}G_a(s)}F_{ext} \\ &= G_{ai}(s)F_{ext} \end{aligned} \tag{17}$$

As shown in Eq. (17), the transfer function $G_{ai}(s)$ has the form of a quadratic delay system. By the inverse Laplace transformation of the transfer function $G_{ai}(s)$, we can obtain the impulse response, as shown in Eq. (18).

$$y(t) = A_1 e^{\lambda_{a+}t} + A_2 e^{\lambda_{a-}t} + A_3 e^{\lambda_{i+}t} + A_4 e^{\lambda_{i-}t} \tag{18}$$

$$\lambda_{a+} = -\frac{D_{d,a}}{2M_{d,a}} + \frac{\sqrt{D_{d,a}^2 - 4K_{d,a}M_{d,a}}}{2M_{d,a}} \tag{19}$$

$$\lambda_{a-} = -\frac{D_{d,a}}{2M_{d,a}} - \frac{\sqrt{D_{d,a}^2 - 4K_{d,a}M_{d,a}}}{2M_{d,a}} \tag{20}$$

$$\lambda_{i+} = -\frac{D_{d,i}}{2(M_{d,i}+m)} + \frac{\sqrt{D_{d,i}^2 - 4K_{d,i}(M_{d,i}+m)}}{2(M_{d,i}+m)} \tag{21}$$

$$\lambda_{i-} = -\frac{D_{d,i}}{2(M_{d,i}+m)} - \frac{\sqrt{D_{d,i}^2 - 4K_{d,i}(M_{d,i}+m)}}{2(M_{d,i}+m)} \tag{22}$$

where $A_1 - A_4$ are time-invariant coefficients that include the mechanical properties ($M_{d,a}, D_{d,a}, etc.$), and the values of the mechanical properties make up λ that determines the response of the system. From Eqs. (19) and (20), when $D_{d,a}^2 - 4K_{d,a}M_{d,a} < 0$, the response obtained by admittance control is an oscillatory solution, but the first term is always negative, so the response is a damped oscillation. If $D_{d,a}^2 - 4K_{d,a}M_{d,a} > 0$, the response is overdamped because $\lambda_{a+} < 0, \lambda_{a-} < 0$, which are not an oscillatory solution. From Eqs. (21) and (22), when $D_{d,i}^2 - 4K_{d,a}(m + M_{d,i}) < 0$, the response is a damped oscillation as in admittance control, and when $D_{d,i}^2 - 4K_{d,a}(m + M_{d,i}) > 0$, the response is overdamped. Because the mass m of the system is in the root sign of the content of $\lambda_{i+}, \lambda_{i-}$, the more accurate the estimation of the mass of the system, the more accurate the selection of damped oscillation and overdamping.

Nyquist diagram

To demonstrate the stability of the control law in the frequency domain, the transfer functions of the admittance control alone, impedance control alone, and the proposed method are obtained. The qualitative stability of the control laws is discussed by obtaining Nyquist diagrams based on transfer functions. Here, the external force is assumed to be a hypothetical spring force. To obtain the transfer function of each control law in this section, the quadratic transfer functions $G_d(s), G_{d,i}(s), and\ G_{d,a}(s)$, which have each mechanical property as a coefficient, are defined as follows

$$G_d(s) = M_d s^2 + D_d s + K_d \tag{23}$$

$$G_{d,i}(s) = M_{d,i} s^2 + D_{d,i} s + K_{d,i} \tag{24}$$

$$G_{d,a}(s) = M_{d,a} s^2 + D_{d,a} s + K_{d,a} \tag{25}$$

The transfer function of each control law is obtained based on Eqs. (23–25). First, using the Laplace transform of Eq. (26), which is a substitution for Eq. (5), into Eq. (1) for impedance control, we can obtain a transfer function whose input is the initial position x_0, and whose output is the current position x; $G_I(s)$ is obtained as shown in Eq. (27).

$$\begin{aligned} m\ddot{x} = &\left(\frac{m}{M_\mathrm{d}} - 1\right) F_\mathrm{ext} \\ &+ m\ddot{x}_0 - \frac{m}{M_\mathrm{d}}(D_\mathrm{d}\dot{e} + K_\mathrm{d}e) - k_e(x - x_0) \end{aligned} \tag{26}$$

$$G_I(s) = \frac{k_e + K_d}{G_d(s) + k_e} \tag{27}$$

Next, for admittance control, Eq. (28) can be obtained by the Laplace transformation Eq. (6).

$$(M_d s^2 + D_d s + K_d) X_d = -k_e X + (K_d + k_e) X_0 \tag{28}$$

Then, Eq. (29) can be obtained by the Laplace transformation of Eq. (8).

$$(ms^2 + k_v s + k_p) X - k_p X_d = -k_e (X - X_0) \tag{29}$$

Finally, by combining Eqs. (28) and (29) and eliminating the intermediate variable X_d, the transfer function $G_A(s)$ of the admittance control is obtained, as shown in Eq. (30).

$$G_A(s) = \frac{k_e G_d(s) + k_p(k_e + K_d)}{(ms^2 + k_p + k_v s + k_e) G_d(s) + k_p k_e} \tag{30}$$

Next, the transfer function of the proposed method was obtained. First, by Laplace transformation of Eqs. (9) and (10), we obtain Eqs. (31) and (32), respectively.

$$\begin{aligned} &(M_{d,a} s^2 + D_{d,a} s + K_{d,a}) X_d \\ &= -k_e (X - X_0) + (M_{d,a} s^2 + D_{d,a} s + K_{d,a}) X_0 \end{aligned} \tag{31}$$

$$\begin{aligned} F = &\left(\frac{m}{M_{d,i}} - 1\right) F_{ext} \\ &+ \frac{m}{M_{d,i}} \{ D_{d,i}(X_d - X)s + K_{d,i}(X_d - X) \} \end{aligned} \tag{32}$$

Now, by combining Eq. (31) and Eq. (32) and eliminating X_d as in the admittance control, we obtain Eq. (33).

$$
\begin{aligned}
F = &- \left(\frac{m}{M_{d,i}} - 1 \right) k_e (X - X_0) \\
&+ \frac{m}{M_{d,i}} (D_{d,i} s + K_{d,i}) \\
&\times \left\{ \left(\frac{-k_e}{G_{d,a}(s)} X + \frac{G_{d,a}(s) k_e}{G_{d,a}(s)} X_0 \right) - X \right\}
\end{aligned} \tag{33}
$$

Finally, by substituting Eq. (33) into the Laplace transform of Eq. (1), the transfer function of the proposed method is expressed by Eq. (34).

$$
G_{AI}(s) = \frac{k_e G_{d,a}(s) + (D_{d,i} s + K_{d,i})(k_e + K_{d,a})}{G_{d,a}(s)(G_{d,i}(s) + k_e) + k_e (D_{d,i} s + K_{d,i})} \tag{34}
$$

Substituting $s = i\omega$ into Eqs. (27, 30, 34) yields the real and imaginary parts of the transfer function in the frequency domain. The real and imaginary parts of each transfer function $G_A(\omega)$, $G_I(\omega)$, and $G_{AI}(\omega)$ for a certain ω are obtained from $\omega : -\infty \rightarrow \infty$, and finally, the Nyquist diagram can be obtained. The Nyquist diagram is shown in Fig. 3.

When $k_e = 10$, which is the top left figure in Fig. 3, the impedance and admittance controls produce the same Nyquist diagram, but the proposed method produces a different one that is enlarged in the imaginary and positive directions of the real axis. In this case, the proposed method does not consider the friction and time delay of the sensor in the calculation of the frequency response. The reason for the expansion of the Nyquist diagram of the proposed method in the imaginary axis direction and positive direction of the real axis is that the admittance-controlled position controller, as shown in Eq. (7), has a high gain, whereas the impedance controller, as the position controller of the proposed method, as shown in Eq. (10), has a low gain owing to the difference between the desired position and the current position. This is because impedance control, as a position controller of the proposed method shown in Eq. (10), provides input via mechanical impedance $(M_{d,i}, D_{d,i}, K_{d,i})$ for the difference between the desired position and the current position, and thus, is less prone to instability.

When $k_e = 300$, which is the top-right panel in Fig. 3, admittance control and impedance control give almost the same Nyquist diagram, indicating that the proposed method has the farthest trajectory from the instability point. Admittance control increases the possibility of instability as the stiffness of the contacting environment increases, and this fact can also be observed, although negligibly, in Fig. 3. The stability of the proposed method is better than that of the other two controllers because impedance control as a position controller is more robust compared to admittance control, as in the case of

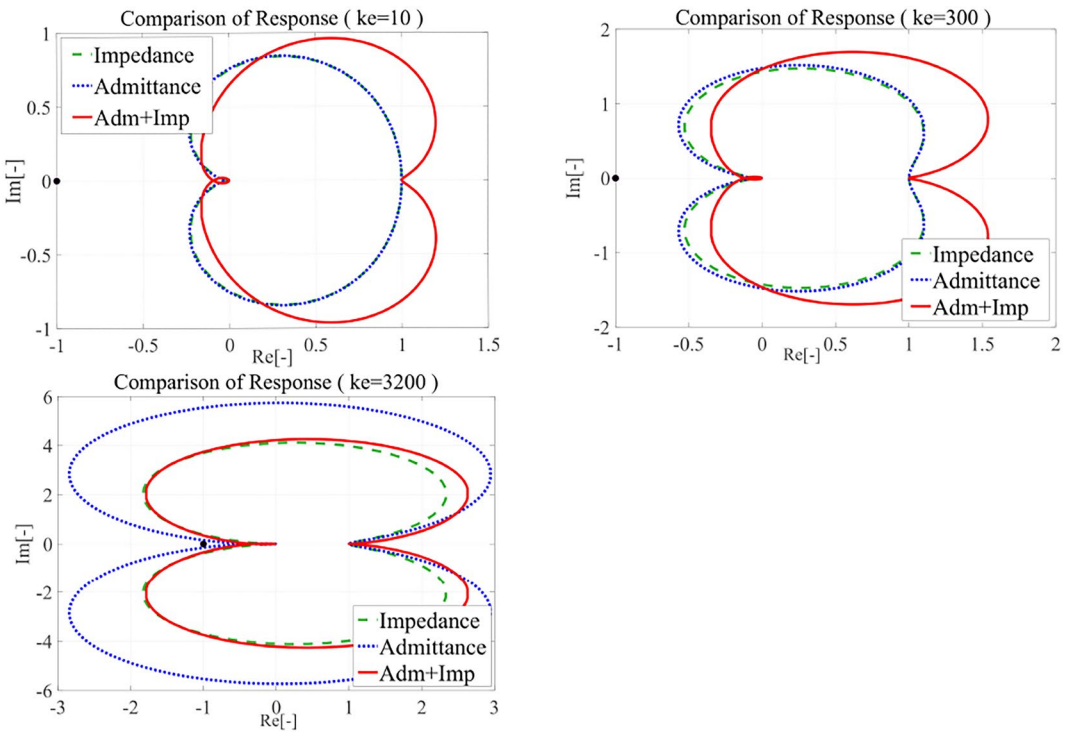

Fig. 3 Comparison of each Nyquist diagram

$k_e = 10$. In the plain admittance controller, the position controller is often set to a high gain to achieve the exact position of the virtual object, but this causes the virtual object to diverge when a large external force acts on it, giving an input that destabilizes the end-effector. However, when compared with the impedance controller only, the proposed method can eliminate the disadvantages of the impedance controller, such as accuracy degradation due to modeling errors, including friction. By calculating the position of the virtual object, which is intentionally different from the original desired position, based on the external force from the contacting environment, the steady-state error due to friction can be reduced, and the modeling error can be absorbed.

When $k_e = 3200$, that is, the bottom left panel in Fig. 3, the closest to the unstable point is the admittance controller. This result is consistent with the fact that the admittance controller becomes unstable when in contact with a rigid environment. This is because the position of the virtual object diverges when a sudden external force is induced by contact with a rigid environment. However, the impedance controller only and the proposed method, both of which are stable against contact with a rigid environment, yielded almost the same Nyquist diagram. Comparing only the admittance controller and the proposed method, one of the terms in the denominator of the transfer function of the admittance controller in Eq. (30) is the sum of the high gain (k_p, k_v), mass of the control object (m), and environmental stiffness (k_e) to realize accurate tracking of admittance control. In contrast, in the proposed method, the product of $G_{d,a}(s)$ and $G_{d,i}(s)$ is used, as can be seen from the first term in the denominator of Eq. (34), which indicates that the number of selectable parameters is increased and by choosing these parameters adequately, a wider range of responses can be realized compared to the admittance controller only. This implies that even when the motion of the virtual object is stiffened (the mechanical property of $G_{d,a}(s)$is increased), softening of the impedance control of the position controller (the mechanical property of $G_{d,i}(s)$ is decreased) can prevent the transfer function from becoming unstable. Equations (30) and (34) are both fourth-order delay system; therefore, there is a possibility of instability subject to the set parameters, but the unstable region is very small, as can be seen in the Nyquist diagram. In contrast, the proposed method in Eq (34) can regulate the time constant of the response in a certain range and avoid instability. In addition, it is possible to realize the desired mechanical response in a wider range compared to that obtained by the impedance or admittance controller only because the mechanical impedance and admittance parameters can be chosen adequately. The most notable point in Fig. 3 is that both the mechanical admittance and impedance specified by the proposed method are constant, even in an environment with changing stiffness. Namely, the Nyquist diagram indicates that stability can be maintained while maintaining the positional accuracy in low-stiffness environments and that instability can be avoided in high-stiffness environments by suppressing vibration through the dynamics of the impedance–controlled part.

Simulation result

The control accuracy of the proposed method was confirmed through numerical simulations on a one-dimensional system. The simulation conditions were equivalent to those used of Ott et al. [18]. The external force acting on the system was modeled as a linear spring, as shown in Eq. (35), and the system is assumed to be subject to the frictional force shown in Eq. (36) in addition to the external force and input. Based on the above conditions, the equation of motion of the system is given as follows:

$$F_{\text{ext}} = -k_e(x - x_0) \tag{35}$$

$$F_{\text{f}} = -\text{sign}(\dot{x})(c_{\text{v}}|\dot{x}| + F_{\text{c}}) \tag{36}$$

$$m\ddot{x} = F + F_{\text{ext}} + F_{\text{f}}. \tag{37}$$

The friction parameters are set to $F_c = 2.0$ and $c_v = 0.5$. The desired mechanical properties set for impedance control only, admittance control only, and the proposed method are listed in Table 1.

Table 1 Each desired mechanical characteristic parameter

	$\boldsymbol{m}$	**0.8**
Impedance control	$\boldsymbol{M_{\text{d}}}$	1.0
	$\boldsymbol{K_{\text{d}}}$	50 or 100 or 200
	$\boldsymbol{D_{\text{d}}}$	$\boldsymbol{2 \times 0.7\sqrt{K_{\text{d}}M_{\text{d}}}}$
	m	0.8
	M_{d}	1.0
Admittance control	K_{d}	50 or 100 or 200
	D_{d}	$2 \times 0.7\sqrt{K_{\text{d}}M_{\text{d}}}$
	k_p	10^6
	k_v	$2 \times 0.7\sqrt{k_p m}$
	m	0.8
	$M_{\text{d,i}}$	1.0
	$K_{\text{d,i}}$	50 or 100 or 200
Proposed control	$D_{\text{d,i}}$	$2 \times 0.7\sqrt{K_{\text{d,i}}M_{\text{d,i}}}$
	$M_{\text{d,a}}$	1.0
	$K_{\text{d,a}}$	$5 \cdot 10^3$or10^4or$2 \cdot 10^4$
	$D_{\text{d,a}}$	$2 \times 0.7\sqrt{K_{\text{d,a}}M_{\text{d,a}}}$

The initial position of the control object is the x-axis origin, as shown in Fig. 1, and $x_0 = 0.10$ is given as the desired position. To ensure the behavior of the linear spring in response to changes in the stiffness of the external environment, three different spring constants, $k_e = 10$, 300, and 3200, were set for comparison. In this study, the force sensor was assumed to be attached to the tip of the control objective, and the simulation was conducted assuming that the force information obtained from the force sensor include a time delay of $T_d = 0.002[s]$ (dead time). The simulations in this section compare the behavior of several mechanical properties for a single environmental stiffness k_e. In the case of impedance control alone, the desired stiffness K_d is chosen among three different values ($K_d = 50, 100, 200$). Similarly, for admittance control alone, the desired stiffness K_d is chosen among three different values ($K_d = 50, 100, 200$), assuming a high-gain position controller. In addition, the proposed method is compared with a total of five types of controllers: one in which the desired stiffness $K_{d,a}$ on the admittance side is chosen among three different values ($K_{d,a} = 50, 100, 200$) while the desired stiffness $K_{d,i}$ on the impedance side is constant, and another in which the desired stiffness $K_{d,i}$ on the impedance side is chosen among two different values ($K_{d,i} = 5000, 20,000$), while the desired stiffness $K_{d,a}$ on the admittance side is constant. The simulation results are shown in Figs. 4, 5, and 6. As shown in Fig. 4, in the low-stiffness environment $k_e = 10$, the performances of the proposed method and admittance control are almost the same. However, the impedance control has a steady deviation, although the deviation becomes smaller as the desired stiffness K_d increases. The reason for this deviation is that the impedance control takes the difference between the desired position and the current position as the input and the force as the output; thus, the system is stationary at the local equilibrium point where the output

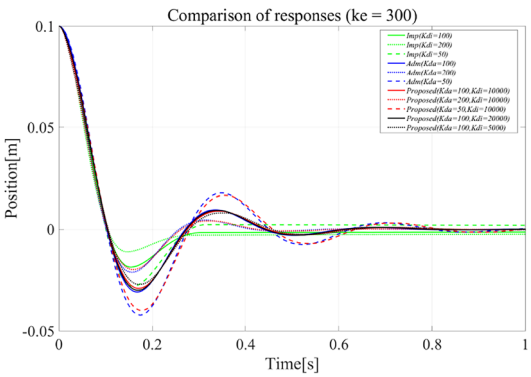

Fig. 5 Transient response of x in $k_e = 300$

force and friction are balanced. However, in admittance control and the proposed method, the virtual desired position x_d is determined only by the external force due to the spring, and no deviation remains because the motion of the virtual object is realized by the final stage position controller.

Next, as can be seen from Fig. 5, the proposed method has the same performance as the admittance control in the medium-stiffness environment $k_e = 300$ as well as in the low-stiffness environment. However, unlike the case of $k_e = 10$, the impedance control had no oscillation, and the impedance control had the smallest overshoot when compared with the same desired stiffness (Imp($K_{d,i} = 200$), Adm($K_{d,a} = 200$), Proposed($K_{d,a} = 200, K_{d,i} = 10,000$) are shown in Fig. 5). The impedance control had the smallest overshoot. This is believed to be because the external force acting on the virtual object increases as the external force acting on the system increases, causing oscillations, and the system follows the oscillations. When the desired viscoelasticity of the impedance control in the final stage

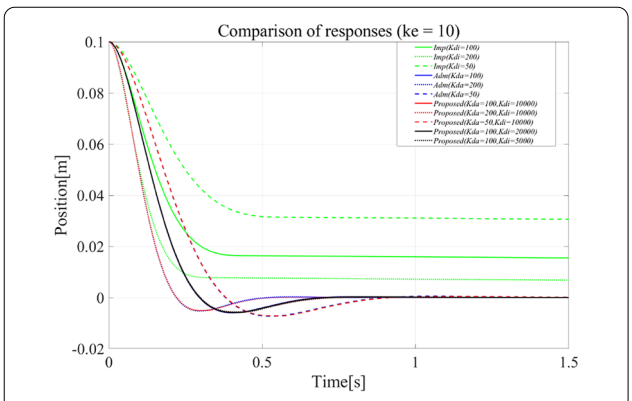

Fig. 4 Transient response of x in $k_e = 10$

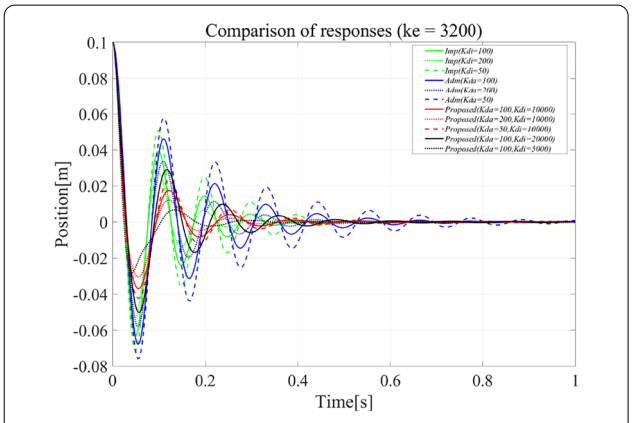

Fig. 6 Transient response of x in $k_e = 3200$

was changed, the system did not follow the oscillation proposed ($K_{d,a} = 100, K_{d,i} = 5000$) in Fig. 5); however, amplitude of the oscillation became larger than that of the impedance control. Although impedance control is better in terms of stability, steady-state deviation occurs when compared with the proposed method and admittance control; thus, it is necessary to select the method according to the task.

Finally, as illustrated in Fig. 6, both the deviation and vibration amplitude were the lowest for the proposed method ($K_{d,a} = 100, K_{d,i} = 5000$) in the highly rigid environment $k_e = 3200$. Owing to the increase in the stiffness of the contacting environment, the vibration of the virtual object in the admittance control increases. Compared with the proposed method and impedance control, the amplitude of admittance control is larger for any desired stiffness. In contrast, because the proposed method uses admittance control, the virtual object diverges just like admittance control alone, but the vibration amplitude of the proposed method is small because the final stage is impedance control, which absorbs the vibration. Both deviations and vibrations are better than those of impedance control, which can be controlled relatively stably in highly rigid environments. This is because the desired position used in the impedance control is obtained from the admittance control, which results in impedance matching between the admittance and impedance controls. In this study, to eliminate deviations and ensure responsiveness, the mechanical characteristics were determined so that the response would be damped oscillation, using the value of λ determined in the stability chapter; as a result, a high vibration suppression effect was obtained by impedance matching.

Experiments on a system with one degree of freedom

Experimental setup

The usefulness of the proposed admittance impedance controller was demonstrated through numerical simulations. However, these results are based on numerical simulation results, and the robustness to friction, time delay, and modeling error, which cannot be completely reproduced by simulations, has not yet been discussed. In this study, fundamental experiments using the proposed admittance impedance controller were conducted using a single degree-of-freedom system, to demonstrate the practicality of the proposed controller. Figures 7 and 8 show the overall image of the experimental setup.

As shown in Fig. 7, a force sensor (LMA-A-100N, Kyowa Dengyo) was attached to the stage of the ball screw (SKR3320B, THK), and a jig was attached so that the external force of the spring acted on the force sensor. The spring constant of each spring used in this research is

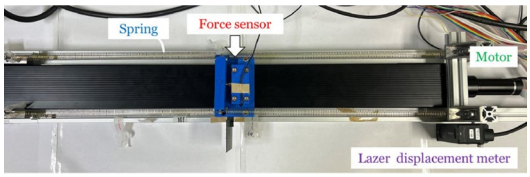

Fig. 7 Picture of an experimental machine with one degree of freedom

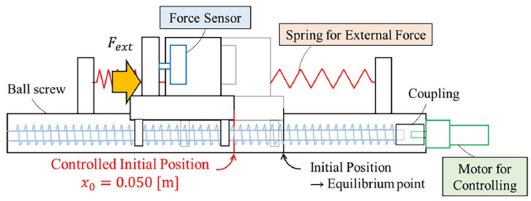

Fig. 8 Schematic of an experimental machine with one degree of freedom

$\hat{k}_e = 6.25, 100$[N/m], and because four equal springs are arranged, the total spring constant is $k_e = 25,400$[N/m]. To realize not only the pulling force but also the pressing force, four springs are arranged with their natural length extended. The gear head (planetary gearhead 32A, Maxon motor) attached to the motor (RE25, Maxon motor) used to drive the ball screw has a reduction ratio of 28:1, and the position of the stage is measured using a lazer displacement meter (IL-1000, Keyence). The flow of the experiment is as follows:

(1) The initial position is the equilibrium point when the four springs attached to the jig.
(2) The robot moves to the starting position of the experiment ($x_0 = 0.050$[m]) within 5 s by controlling the position using a motor.
(3) Four seconds after the start of the experiment, the force is controlled at the equilibrium point under the external force.

In this study, a digital signal processing system (SEAGULL mini, MIS) is used as the controller, and the control period was 0.33[ms]. The control program was written in MATLAB.

Experimental result

The controllers to be compared are as follows: Eq. (5) for the impedance controller, Eqs. (6) and (7) for the admittance controller, and Eqs. (9) and (10) for the proposed admittance–impedance controller. The mechanical properties of each are listed in Table 2.

Table 2 Mechanical properties of each controller for experiments

Parameter		Value
Impedance control	m	0.8
	M_d	1.0
	K_d	10^3
	D_d	$2 \times 0.7\sqrt{K_d M_d}$
Admittance control	m	0.8
	M_d	1.0
	K_d	200
	D_d	$10\sqrt{K_d M_d}$
	k_p	3×10^4
	k_v	$2 \times 0.7\sqrt{k_p m}$
Proposed control	m	0.8
	$M_{d,i}$	0.6
	$K_{d,i}$	3×10^4
	$D_{d,i}$	$2 \times 0.7\sqrt{K_{d,i} M_{d,i}}$
	$M_{d,a}$	1.0
	$K_{d,a}$	200
	$D_{d,a}$	$10\sqrt{K_{d,a} M_{d,a}}$

The response at $k_e = 25$ is illustrated in Fig. 9. The response at $k_e = 400$ is shown in Fig. 10. As can be seen from Figs. 9 and 10, the desired position ($x_0 = 0.050$[m]) was reached in the first 5 [s] of position control. In Fig. 9, after 5.0[s], there was not much difference in the response between the admittance control (blue line) and the proposed method (red line); however, the impedance control (green line) converged slowly to the desired position and left a steady deviation. The reason for the remaining steady-state deviation in the impedance control is thought to be the effect of static friction, which was not considered in the modeling stage. As can be seen from Eq. (5), the impedance control outputs a force based on the difference between the current position and the desired position as input. The larger the difference between the current position and the desired position, the larger the force. Therefore, as the desired position is approached, the input becomes smaller, and the force from the motor to the ball screw is balanced by the static friction force, resulting in settling at the local equilibrium point. Although there is no oscillation as in the admittance control and the proposed method, the continuous deviation is a disadvantage from the viewpoint of both accuracy and stability. In contrast, admittance control and the proposed method have a better response to the desired position than impedance control, and converge to the target position without deviation, although there are some oscillations. As can be seen from Eqs. (6) and (9), the admittance control and the proposed method output the virtual desired position x_d using only the external force owing to the spring force as an input, and no deviation is generated owing to the position control that does not consider the effect of friction. However, when the virtual object vibrates owing to the external force acting on the spring, this effect is noticeable. As shown in Fig. 9, the vibration amplitude of the proposed method was slightly smaller than that of admittance control. For $k_e = 25$, the proposed method has the same accuracy as admittance control, which is superior in low-stiffness environments. Next, as can be seen from Fig. 10, even at $k_e = 400$, the vibration amplitude of the proposed method is smaller than that of the admittance control when compared with the proposed method. Although the responses to the desired position are comparable, the proposed method is more responsive than impedance control. However, impedance control is the best at suppressing the vibration near the desired position, followed by the proposed

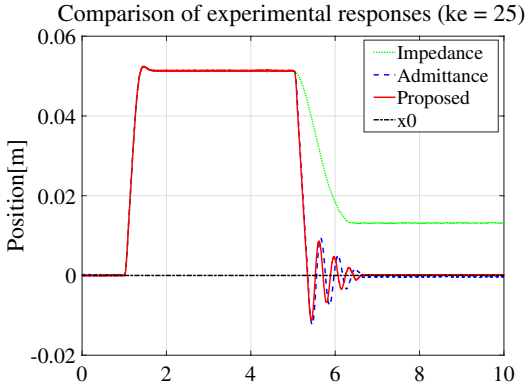

Fig. 9 Transient response of displacement of the control object (ke = 25)

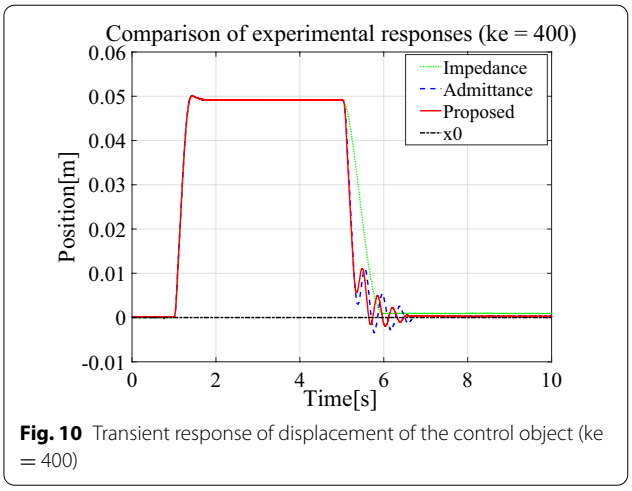

Fig. 10 Transient response of displacement of the control object (ke = 400)

method. This is because, as mentioned in the case of $k_e = 25$, the proposed method and the admittance control show the effect of the vibration of the virtual object on the response. In impedance control, the more accurate the modeling is, the less is the influence of external forces on the control law, and thus, the smaller the oscillations are even when a large external force acts. In terms of the stability comparison, it can be observed that impedance control performs the best. However, as shown in Fig. 10, deviation of the impedance control is larger than that of the proposed method and the admittance control. There is a tradeoff between positional accuracy and stability, and the priority depends on the task. Impedance control is better for avoiding the instability caused by vibration, whereas the proposed method is better at achieving a high response and accuracy.

Force control in a two-dimensional model

Only a one-dimensional case study is insufficient when controlling a multi-articulated manipulator. Here, we extend the proposed method to a two-dimensional case using a two-dimensional manipulator model. The proposed admittance impedance controller is verified in terms of the features compared with the conventional force controllers. Moreover, a parameter design method is proposed to achieve the intended operation of the operator by designing the mechanical characteristics of admittance control and impedance control parts.

Two-dimensional model

In this study, the two-dimensional manipulator model with two joints is considered, which is shown in Fig. 11. Unlike the one-dimensional case, the range of motion of the manipulator is planar so that the stiffness of the manipulator must be designed in two-dimensions, according to the desired task. To consider the contact task, we assume that the manipulator unconsciously contacts the environment during movement. The equation of motion of the two-dimensional manipulator model when the end-effector contacts the environment is as follows:

$$\boldsymbol{M}_q\ddot{\boldsymbol{q}} + \boldsymbol{h}_q = \boldsymbol{\tau} - \boldsymbol{A}^{\mathrm{T}}\boldsymbol{\lambda}, \tag{38}$$

where $\boldsymbol{q} = [q_1\ q_2]^{\mathrm{T}}$ denotes the angle of each joint of the manipulator, $\boldsymbol{M}_q$ denotes the inertia matrix of the manipulator, $\boldsymbol{h}_q$ denotes a nonlinear term including gravity and Coriolis force, $\boldsymbol{A} = \frac{\partial \Phi}{\partial \boldsymbol{q}}$ denotes the constraint Jacobian matrix when the end-effector contacts the environment, $\boldsymbol{\lambda}$ denotes the constraint force (this is a different value from the eigenvalue in stability), and $\boldsymbol{\tau}$ denotes the input torque applied to each joint. The geometric constraint condition is that the tip of the end-effector must not penetrate the inside of the contacting object, such that $\Phi = z - z_s$, and z_s is the z-coordinate of the plane. The constraint stabilization method (CSM) [21] was used to guarantee stability of the simulations. The equation for the geometric constraint condition Φ is Eq. (39).

$$\ddot{\Phi} + \alpha\dot{\Phi} + \beta\Phi = 0 \tag{39}$$

where α and β are CSM coefficients that maintain the stability of the simulation; in this study, we used $\alpha = 1.4\sqrt{\beta}$ and $\beta = 10^4$. The first and second derivatives of Φ are expressed in Eqs. (40) and (41), respectively.

$$\dot{\Phi} = \frac{\partial \Phi}{\partial \boldsymbol{q}}\dot{\boldsymbol{q}} \tag{40}$$

$$\ddot{\Phi} = \frac{\mathrm{d}}{\mathrm{d}t}\left(\frac{\partial \Phi}{\partial \boldsymbol{q}}\right)\dot{\boldsymbol{q}} + \frac{\partial \Phi}{\partial \boldsymbol{q}}\ddot{\boldsymbol{q}} \tag{41}$$

By substituting Eqs. (40) and (41) into Eq. (39), Eq. (39) can be transformed into Eq. (42).

$$\frac{\partial \Phi}{\partial \boldsymbol{q}}\ddot{\boldsymbol{q}} + \left\{\alpha\frac{\partial \Phi}{\partial \boldsymbol{q}} + \frac{\mathrm{d}}{\mathrm{d}t}\left(\frac{\partial \Phi}{\partial \boldsymbol{q}}\right)\right\}\dot{\boldsymbol{q}} + \beta\boldsymbol{\Phi} = 0 \tag{42}$$

The extended equation of motion of the manipulator is as shown in Eq. (43) by combining the constraint equation (Eq. (42)) for the numerical simulations.

$$\begin{bmatrix} \boldsymbol{M}_q & \boldsymbol{A}^{\mathrm{T}} \\ \frac{\partial \Phi}{\partial \boldsymbol{q}} & O \end{bmatrix}\begin{bmatrix} \ddot{\boldsymbol{q}} \\ \lambda \end{bmatrix} + \begin{bmatrix} \boldsymbol{h}_q \\ \left\{\alpha\frac{\partial \Phi}{\partial \boldsymbol{q}} + \frac{\mathrm{d}}{\mathrm{d}t}\left(\frac{\partial \Phi}{\partial \boldsymbol{q}}\right)\right\}\dot{\boldsymbol{q}} + \beta\Phi \end{bmatrix} = \begin{bmatrix} \boldsymbol{\tau} \\ O \end{bmatrix} \tag{43}$$

The admittance impedance controller in two dimensional case

We compared the proposed method with the admittance controller only and the impedance controller only, similar to the verification of the one-dimensional model case.

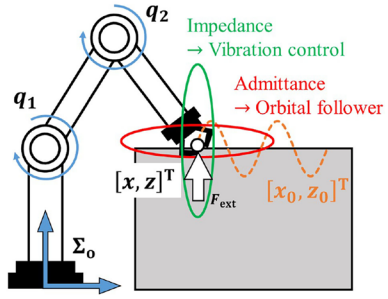

Fig. 11 Control object (two-dimensional manipulator)

The inputs for the admittance control and impedance control are shown in Eqs. (44) and (45), and the inputs for the proposed admittance impedance controller in two dimensions are expressed in Eq. (46).

Admittance controller

$$\begin{aligned} &\boldsymbol{M}_{\mathrm{a}}\ddot{\boldsymbol{X}}_{\mathrm{d}} + \boldsymbol{D}_{\mathrm{a}}\dot{\boldsymbol{X}}_{\mathrm{d}} + \boldsymbol{K}_{\mathrm{a}}(\boldsymbol{X}_{\mathrm{d}} - \boldsymbol{X}_0) = \boldsymbol{F}_{\mathrm{ext}} \\ &\boldsymbol{\tau} = -\boldsymbol{J}^{\mathrm{T}}\left(\boldsymbol{k_d}\left(\dot{\boldsymbol{X}}_{\boldsymbol{d}} - \dot{\boldsymbol{X}}\right) + \boldsymbol{k_p}(\boldsymbol{X_d} - \boldsymbol{X})\right) \end{aligned} \tag{44}$$

Impedance controller

$$\boldsymbol{\tau} = -\boldsymbol{J}^{\mathrm{T}}\left(\boldsymbol{D_i}\left(\dot{\boldsymbol{X}} - \dot{\boldsymbol{X}}_{\boldsymbol{0}}\right) + \boldsymbol{K_i}(\boldsymbol{X} - \boldsymbol{X_0})\right) \tag{45}$$

Admittance impedance controller

$$\begin{aligned} &\boldsymbol{M}_{\mathrm{d,a}}\ddot{\boldsymbol{X}}_{\mathrm{d}} + \boldsymbol{D}_{\mathrm{d,a}}\dot{\boldsymbol{X}}_{\mathrm{d}} + \boldsymbol{K}_{\mathrm{d,a}}(\boldsymbol{X}_{\mathrm{d}} - \boldsymbol{X}_0) = \boldsymbol{F}_{\mathrm{ext}} \\ &\boldsymbol{\tau} = -\boldsymbol{J}^{\mathrm{T}}\left(\boldsymbol{D_{d,i}}\dot{\hat{\boldsymbol{e}}}_{\boldsymbol{d}} + \boldsymbol{K_{d,i}}\hat{\boldsymbol{e}}_{\boldsymbol{d}}\right) \end{aligned} \tag{46}$$

where $\hat{\boldsymbol{e}}_d = \boldsymbol{X}_d - \boldsymbol{X}$, $\boldsymbol{X}$ denotes the tip position of the end-effector, $\boldsymbol{X}_d$ denotes the virtual object position derived from the admittance controller, $\boldsymbol{X}_0$ denotes the desired position, and $\boldsymbol{J}$ denotes the Jacobian matrix of the manipulator. As a control flow, the position and velocity of the virtual object are derived by the admittance controller, and the position and velocity of the virtual object are used as reference positions and velocity in the impedance controller; the position and velocity of the end-effector are regulated according to the virtual dynamics of the impedance controller. The advantage of the proposed method is that the mechanical properties of admittance control and impedance control can be designed individually; thus, the behavior of the manipulator can be designed according to the required task. As an example, we show that, given the desired trajectory that differs from the information on the object's surface, the desired trajectory can be followed in the horizontal direction without applying excessive force.

The mechanical properties of the admittance controller, impedance controller, and the proposed method used in the simulations are shown in Eq. (47). Figure 11 shows an image of the stiffness ellipse determined based on the mechanical properties.

$$\begin{aligned} &\boldsymbol{M}_{d,a} = \boldsymbol{M}_{d,i} = \begin{bmatrix} 1.0 & 0 \\ 0 & 1.0 \end{bmatrix}, \\ &\boldsymbol{K}_a = \begin{bmatrix} 10^4 & 0 \\ 0 & 10^3 \end{bmatrix}, \boldsymbol{K}_{d,a} = \begin{bmatrix} 10^4 & 0 \\ 0 & 10^3 \end{bmatrix}, \\ &\boldsymbol{K}_{d,i} = \boldsymbol{K}_i = \begin{bmatrix} 10^3 & 0 \\ 0 & 10^4 \end{bmatrix}, \boldsymbol{k}_p = \begin{bmatrix} 10^5 & 0 \\ 0 & 10^5 \end{bmatrix}, \\ &\boldsymbol{k}_d = \begin{bmatrix} 1.05 \times 10^3 & 0 \\ 0 & 1.05 \times 10^3 \end{bmatrix}, \\ &\boldsymbol{D}_{d,a} = \boldsymbol{D}_a = \begin{bmatrix} 10^2 & 0 \\ 0 & 10^2 \end{bmatrix}, \\ &\boldsymbol{D}_i = \begin{bmatrix} 5.0 \times 10^2 & 0 \\ 0 & 10^3 \end{bmatrix}, \boldsymbol{D}_{d,i} = \begin{bmatrix} 10^2 & 0 \\ 0 & 5.0 \times 10^2 \end{bmatrix}, \end{aligned} \tag{47}$$

As can be seen from Eq. (47), the admittance controller increases the stiffness in the x-direction to increase the ability to follow the desired trajectory, and the impedance controller increases the stiffness in the z-direction to allow for flexibility perpendicular the plane. In the admittance control part of the proposed method, the stiffness in the x-direction of the admittance control part is increased to suppress vibrations and excessive pushing forces associated with contact while improving the tracking to the desired trajectory; in the impedance control part of the proposed method, the stiffness in the z-direction is also increased. As an eventual advantage of the proposed method, the impedance control part can eliminate the vibration at the time of contact with the environment, which is a disadvantage of the admittance control part, while incorporating the advantage of the high follow-up capability of the admittance controller.

Two demensional simulation

In this study, to demonstrate the practicality of the proposed method, we evaluated the suppression of the generated vibrations and the ability to follow them in the x-direction by providing trajectories that run into the plane. The desired position $\boldsymbol{X}_0$, as described in the previous section, is given by Eq. (48).

$$\boldsymbol{X}_0 = \begin{bmatrix} x_0 \\ z_0 \end{bmatrix} = \begin{bmatrix} 0.1 \times t \\ 0.2 \times \sin(2\pi t/5) + z_s \end{bmatrix}, \tag{48}$$

where z_s is the z-coordinate of plane. As shown in Eq. (48), we confirmed the behavior of an end-effector at the time of contact by giving it a desired trajectory that was depressed in the plane with the passage of time. For simplicity, it was assumed that there was no friction.

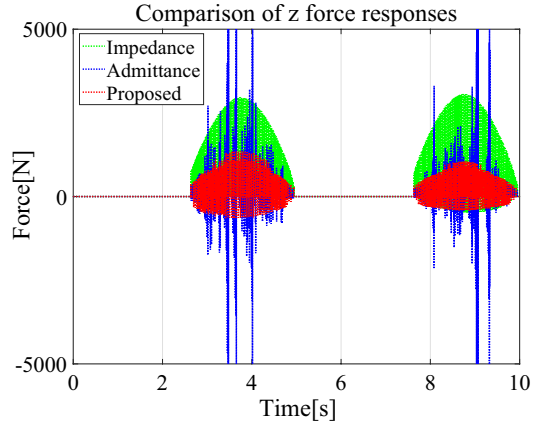

Fig. 14 Time variation of the reaction force in the *z* direction for the three control laws

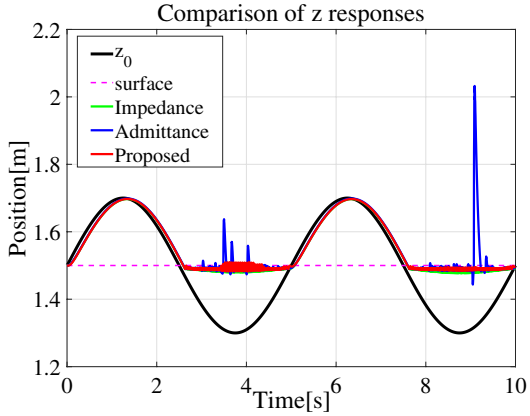

Fig. 13 Transient response of the *z* coordinate of endpoint

Simulation result of two-dimension

Figures 12, 13, and 14 show the simulation results. In Fig. 12, x_0 represents the x-axis component of the desired position. The displacement in the x-direction can be followed almost without error in all control laws. However, in the admittance controller, some oscillation was observed owing to the effect of the contact. By contrast, the proposed method, which generates trajectories considering the reaction force in the admittance control part shows stable behavior without oscillation as in the impedance control. This is because the position controller in the last stage is impedance-controlled. Due to the dynamics of the impedance control part, the oscillation of the admittance-controlled virtual object does not directly affect the behavior.

In Fig. 13, z_0 represents the z component of the desired position. As for the displacement in the z-component, all controllers have the same tracking performance of $0 \sim 2.5$[s]. However, at $2.5 \sim 5.0$[s], the admittance controller shows a large oscillation. In contrast, the impedance controller traces the surface of the object (surface= 1.5[m]) without any oscillation. In addition, the proposed method generates more oscillations than the impedance controller, but not as many as the admittance controller. This is because the position controller in the admittance controller has a high gain and follows the oscillation of the virtual object with high accuracy. This behavior is thought to be caused by the large reaction force generated when the object makes contact with the surface, causing the end-effector to jump up from the surface and then receive a large reaction force again when it attempts to return to its desired trajectory. However, in the impedance controller, the reaction force of the contact is not reflected. In the impedance controller, the spring-damper system with the mechanical impedance parameters (D_i, K_i) used here is controlled only with the error from the desired trajectory as an input. It is thought that the system exhibits stable behavior because only the input to the desired trajectory is given. In the proposed method, the admittance control part is used; however, because the position controller in the final stage is impedance-controlled, it is thought that the vibration is reduced by the virtual dynamics of the impedance control part. Owing to the difference in the degrees of freedom of design within the range from ensuring the trajectory tracking performance, the transmission is suppressed by deliberately setting the mechanical impedance in the impedance control part.

Finally, in Fig. 14, the z-component of the force acting on the end-effector f_z with the three controllers is compared. As for the reaction force in the z-component, it can be observed that the oscillation in the admittance controller causes a large reaction force. In addition, when the proposed method is compared with the impedance controller alone, the proposed method receives only approximately half of the reaction force compared to the

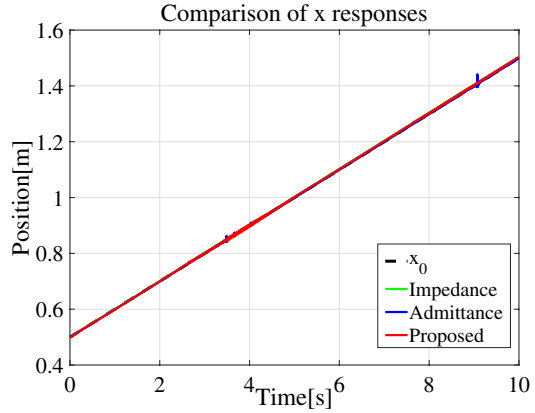

Fig. 12 Transient response of the *x* coordinate of endpoint

impedance controller. This means that the larger the difference from the desired trajectory, the larger the output force becomes because the impedance controller outputs the force based on the difference from the desired trajectory as an input. In contrast, by reducing the mechanical impedance of the impedance controller, the proposed method can achieve the same trajectory-following performance with a low reaction force. This is owing to the effect of the virtual desired position design based on the reaction force at the contact in the admittance controller. By setting the virtual desired position to a position between the actual desired position and the surface of the object based on the reaction force, an excessive reaction force can be avoided. The proposed method is useful because excessive force on the object may damage the object and manipulator.

These results show that the proposed method is capable of generating an interaction force constrained to the selected boundaries for the interaction, even when the surface shape of the object and the desired trajectory are different from those of other force controllers with similar tracking performance.

Conclusion

In this study, we proposed a new force control method, which is a series connection of the admittance and impedance controller, and showed its stability and parameter setting guidelines by Laplace transform and stability in frequency response by Nyquist diagrams. The effectiveness of the proposed method was demonstrated through simulations and experiments using a one-dimensional system, and its extendibility to multiple dimensions was demonstrated through simulations using a sagittal two-degree-of-freedom manipulator model. The results illustrated the improvement in the safety of the robot in tasks in which contact with the external environment is possible and are expected to provide safe and highly accurate control in cooperative tasks between humans and robots. In future work, it will be necessary to validate the effectiveness of the proposed method for a multi-degrees-of-freedom system such as an integrated serial-link manipulator from both theoretical and experimental viewpoints.

Acknowledgements
Funding from Yaskawa Electric Corporation is gratefully acknowledged.

Author contributions
TF designed and executed the experiments and wrote the manuscript. KT is a supervisor and contributed to the concept and edited the manuscript. Both authors read and approved the final manuscript.

Funding
This research was funded by Yaskawa Electric Corporation.

Availability of data and materials
The datasets used and/or analysed during the current study are available from the corresponding author on reasonable request.

Declarations

Ethics approval and consent to participate
Not applicable.

Consent for publication
Not applicable.

Competing interests
This study received funding from Yaskawa Electric Corporation. The funder had the following involvement with study: the study analysis.

Received: 26 April 2022 Accepted: 13 November 2022
Published online: 09 December 2022

References

1. Yi S, Shuang S, Xinquan L, Hongliang R (2016) A miniature soft robotic manipulator based on novel fabrication methods. IEEE Robot Autom Lett 1(2):617–623
2. Michele G, Federico R, Gabriele F, Cecilia L (2013) A Feed-Forward Neural Network Learning the Inverse Kinetics of a Soft Cable-Driven Manipulator Moving in Three-Dimensional Space. In: Proceedings of the 2013 IEEE/RSJ International Conference on Intelligent Robots and Systems, p 5033–5039
3. Michele G, Federico R, Marcello C, Andrea A, Gabriele F, Cecilia L (2012) A two dimensional inverse kinetics model of a cable driven manipulator inspired by the Octopus Arm. In: Proceedings of the 2012 IEEE International Conference on Robotics and Automation, p 3819–3824
4. Federico R, Michele G, Marcello C, Matteo C, Cecilia L (2014) Dynamic model of a multibending soft robot arm driven by cables. IEEE Trans Robotics 30(5):1109–1122
5. Giannaccini EM, Georgilas I, Horsfield I, Peiris HB, Lenz A, Pipe GA, Dogramadzi S (2014) A variable compliance, soft gripper. Autonom Robots 36(1–2):93–107
6. Chen G, Guo S, Hou B, Wang J (2020) Fractional order impedance control. IEEE Access 8:48904–48916
7. Kang G, Oh SH, Seo KJ, Kim U, Choi RH (2019) Variable admittance control of robot manipulators based on human intention. IEEE/ASME Trans Mechatr 24(3):1023–1032
8. Alexandre L, Boris M, Clement G (2012) Variable admittance control of a four-degree-of-freedom intelligent assist device. In: Proceedings of the 2012 IEEE International Conference on Robotics and Automation, pp 3903–3908
9. Landi C T, Ferraguti F, Sabattini L, Secchi C, Fantuzzi C (2017) Admittance Control Parameter Adaptation for Physical Human-Robot Interaction. In: Proceedings of the 2017 IEEE International Conference on Robotics and Automation, pp 2911–2916
10. Kronander K, Billard A (2016) Stability considerations for variable impedance control. IEEE Trans Robotics 32(5):1298–1305
11. Lu WS, Meng QH (1991) Impedance control with adaptation for robotic manipulations. IEEE Trans Robot Autom 7(3):408–415
12. Park HJ, Chung H (1999) Hybrid control for biped robots using impedance control and computed-torque control. In: Proceedings of the 1999 IEEE International Conference on Robotics and Automation, pp 1365–1370
13. Biagiotti L, Liuz H, Hirzinge ZG, Melchiom C (2003) Cartesian Impedance Control for Dexterous Manipulation. In: Proceedings of the 2003 IEEE/RSJ International Conference on Intelligent Robotics and Systems, pp 3270–3275
14. Yoo S, Lee W, Chung KW (2014) Impedance control of hydraulic actuation systems with inherent backdrivability. IEEE/ASME Trans Mechatronics 24(5):1921–1930
15. Kikuuwe R (2019) Torque-bounded admittance control realized by a set-valued algebraic feedback. IEEE Trans Robotics 35(5):1136–1149

16. Yao B, Zhou Z, Wang L, Xu W, Liu Q, Liu A (2018) Sensorless and adaptive admittance control of industrial robot in physical human–robot interaction. Robotics Computer-Integrat Manufact 51:158–168
17. Chen HW, Yang J, Guo L, Li S (2016) Disturbance-observer-based control and related methods - an overview. IEEE Trans Indus Electr 63(2):1083–1095
18. Ott C, Mukherjee R, Nakamura Y (2015) A hybrid system framework for unified impedance and admittance control. J Intell Robotic Syst 78:359–375
19. Anderson RJ, Spong MW (1988) Hybrid impedance control of robotic manipulators. IEEE Int Conf Robotics Autom 4(5):549–556
20. Kaneko T, Ogata K, Sakaino S, Tsuji T (2015) Impact Force Control Based on Stiffness Ellipse Method Using Biped Robot Equipped with Biarticular Muscles. In: Proceedings of the 2015 IEEE/RSJ International Conference on Intelligent Robotics and Systems, pp 2246–2251
21. Baumgarte J (1972) Stabilization of constraints and integrals of motion in dynamical systems. Computer Methods Appl Mech Eng 1:1–16

Publisher's Note